Coulomb Dissociation of ^{19}C and its Halo Structure

T. Nakamura,[1,*] N. Fukuda,[1] T. Kobayashi,[2] N. Aoi,[1] H. Iwasaki,[1] T. Kubo,[3] A. Mengoni,[3,†] M. Notani,[3] H. Otsu,[2] H. Sakurai,[3] S. Shimoura,[4] T. Teranishi,[3] Y. X. Watanabe,[1] K. Yoneda,[1] and M. Ishihara[1,3]

[1]*Department of Physics, University of Tokyo, 7-3-1 Hongo, Bunkyo, Tokyo 113-0033, Japan*

[2]*Department of Physics, Tohoku University, 2-1 Aoba, Aramaki, Aoba, Sendai 980-8578, Japan*

[3]*The Institute of Physical and Chemical Research (RIKEN), 2-1 Hirosawa, Wako, Saitama 351-0198, Japan*

[4]*Department of Physics, Rikkyo University, 3-34-1 Nishi-Ikebukuro, Toshima, Tokyo 171-8501, Japan*

(Received 25 February 1999)

The extremely neutron-rich nucleus ^{19}C has been studied by Coulomb dissociation into $^{18}\mathrm{C} + n$ at 67 A MeV. A large $E1$ strength of $0.71 \pm 0.07\ e^2\,\mathrm{fm}^2$ has been observed at low excitation energies. An analysis of the angular distribution of $^{18}\mathrm{C} + n$ center of mass has led to a determination of the neutron separation energy of ^{19}C to be 530 ± 130 keV. The $E1$ strength distribution can be well reproduced for a ^{19}C ground state structure with a dominant s-wave valence neutron, providing a consistent picture of the neutron halo structure of ^{19}C.

PACS numbers: 25.60.Gc, 21.10.Gv, 25.70.De, 27.20.+n

Halo nuclei have been found in the light and extremely neutron-rich region of the nuclear chart, and have a novel twofold structure composed of a core with normal nuclear density and a halo with diffuse valence neutron(s) [1,2]. The formation of a neutron halo is ascribed basically to the tunneling of the loosely bound valence neutron(s) through the potential well. One unique feature of halo nuclei is a greatly enhanced $E1$ strength at low excitation energies, as revealed in the Coulomb dissociation of ^{11}Be [3,4] and ^{11}Li [5–8].

Coulomb dissociation has been a useful spectroscopic tool for investigating halo structure [1,2]. Coulomb dissociation is a process in which a projectile passes a high-Z target, is excited by absorption of a virtual photon from the changing target Coulomb field, and decays into a breakup channel involving a few particles. The dissociation cross section is related to the electromagnetic transition matrix element $B(E\lambda)$ which contains information on the structure of the projectile ground state [9,10]. For halo nuclei, the $B(E1)$ distribution is simply described as a Fourier transform of $rR(r)$, with r being a distance between the core and halo and $R(r)$ the radial component of the wave function of the halo neutron [11]. The high value of $|R(r)|^2$ at large r in a halo nucleus thus leads to the large $E1$ strength at low excitation energies. The $B(E1)$ distribution can thus be used to determine the wave function of the halo neutron [3,12].

In this work we have studied the ground state structure of ^{19}C by means of Coulomb dissociation. This nucleus has been considered as a promising candidate for a halo nucleus because of the small neutron binding of its ground state. In fact, the adopted one-neutron separation energy S_n is only 160 ± 110 keV [13]. This value is even smaller than that of ^{11}Be ($S_n = 504 \pm 6$ keV), which is the only nucleus where a one-neutron halo structure is well established. Another important factor to dictate the halo property is the orbital angular momentum carried by the outmost valence neutron. According to the standard shell model, the valence neutron of ^{19}C is expected to occupy either an s or d orbital [14–16]. However, the formation of the halo depends strongly on which of these orbitals is occupied by the neutron. Because of the absence of a centrifugal barrier the halo can favorably develop for an s-wave neutron while it will be considerably suppressed by the barrier for a d-wave neutron. Thus the spin-parity of the state as well as the configuration of the wave function is essential for the manifestation of the halo phenomena.

The structure of ^{19}C has so far been investigated by inclusive measurements of either ^{18}C [14,15,17] or the neutron [18] momentum components following the ^{19}C breakup. The momentum distribution of ^{18}C at 77 A MeV [14,15] exhibited a narrow width of 42 ± 4 MeV/c, while that measured at 914 A MeV [17] had a broader width of 69 ± 3 MeV/c. The discrepancy between these measurements has not yet been clearly understood, leaving open the question of the ground state structure itself. For example, Ref. [14] argued for a $J^\pi = 1/2^+$ assignment for the ^{19}C ground state, and indicated halo formation arising from a large component of the $^{18}\mathrm{C}(0^+) \otimes 2s_{1/2}$ configuration. However, the revised analysis [15] suggested the $J^\pi = 5/2^+$ assignment with a large portion of a $^{18}\mathrm{C}(2^+) \otimes 2s_{1/2}$ configuration. The halo formation should be strongly suppressed for this configuration because of the effective increase of S_n by 1.62 MeV corresponding to the cost for the core excitation energy of the $^{18}\mathrm{C}(2^+)$ state. Summing up, the nature of the ^{19}C halo structure still remains unclear. The difficulty in resolving the problem may primarily be attributed to the missing assignment of the spin-parity and also to the possible uncertainty in the mass measurements which yielded the S_n values ranging from 700 keV to nearly 0 keV [13].

In the present Letter we report on the results of a kinematically complete measurement of Coulomb dissociation of ^{19}C at 67 A MeV. Such a measurement has been proven to be powerful to explore ground state

 0031-9007/99/83(6)/1112(4)$15.00

properties of the projectile nucleus [3,6–8,19]. We show that the spin-parity as well as the configuration of the ground state has been determined. Furthermore an S_n value has been obtained from an analysis on the angular distribution. The newly determined S_n value turns out to be crucial for consistent understanding of the ground state properties of ^{19}C.

The experiment was performed at the RIPS facility [20] at RIKEN. The ^{19}C secondary beam was produced by the ^{9}Be(^{22}Ne, ^{19}C)X reaction at 110 A MeV. The ^{19}C beam at $(67 \pm 8)A$ MeV with a typical intensity of 300 counts/sec bombarded a 320-mg/cm^2-thick Pb target. In addition, a 180-mg/cm^2-thick C target was used to estimate contributions arising from nuclear breakup. Background corrections were obtained from a run with no target. The energy of the incident ^{19}C ion was obtained by a TOF (time of flight) measurement using two thin plastic scintillators. The trajectory of ^{19}C was determined by four sets of multiwire proportional chambers.

The breakup particles, ^{18}C and n, emerged in a narrow cone at forward angles with velocities close to that of the ^{19}C projectile. The neutron was detected by four layers of neutron hodoscope arrays with an effective area of 1.08(W) $\times$ 0.86(H) m^2 placed 4.2 m downstream of the target. Each array contained 14 plastic scintillator rods with 6 cm thickness. The angular coverage ranged from -3.7° to 10.8° in the horizontal direction, and from -6.0° to 5.6° in the vertical direction. The neutron momentum vector was determined from the TOF and position information in the arrays. The momentum resolution $\Delta p/p$ (1σ) of neutron was about 0.7%. The intrinsic detection efficiency 18.7% for the threshold energy 8.0 MeV (electron-equivalent energy) was obtained from a separate experiment using the ^{7}Li$(p,n)^{7}$Be reaction at 70 MeV. The corresponding ^{18}C particle was analyzed by a magnetic spectrometer equipped with a drift chamber and plastic scintillator hodoscopes. Particle identification was performed by combining ΔE, TOF data from the hodoscopes, and magnetic rigidity information. The momentum vector of ^{18}C was deduced by the combination of TOF and tracking analysis. The momentum resolution (1σ) of ^{18}C was about 1.3%.

Figure 1(a) shows the dissociation cross sections for the Pb and C targets as a function of the neutron-^{18}C relative energy, $E_{\rm rel}$, which is related to the excitation energy, $E_{\rm x}$, of the projectile by $E_{\rm rel} = E_{\rm x} - S_n$. The integrated breakup cross sections for the Pb and C targets were 1.34 $\pm$ 0.12 b and 82 $\pm$ 14 mb, respectively. The cross section for the Pb target is substantially larger than that for the C target, indicating the dominance of Coulomb dissociation for the Pb target.

The Coulomb dissociation part of the breakup cross section for the Pb target was obtained by subtracting the nuclear contribution scaled from the data for the C target. Here, we assumed that the breakup cross section for the C target was entirely due to the nuclear contribution and the nuclear component of the Pb data scales with that for the C target by the ratio of the (projectile + target) radii. The Coulomb dissociation spectrum thus deduced [Fig. 1(b)] is typical for the breakup of a halo nucleus, showing enhanced cross sections peaked at a low energy ($E_{\rm rel} \cong 300$ keV). The integrated Coulomb dissociation cross section was 1.19 $\pm$ 0.11 b.

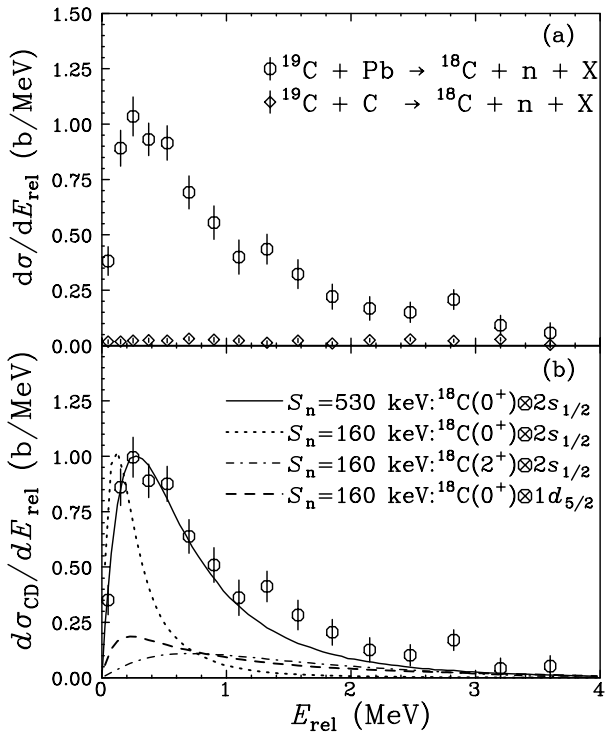

FIG. 1. (a) Dissociation cross sections as a function of relative energy $E_{\rm rel}$ for Pb (circles) and C (diamonds) targets. (b) Coulomb dissociation cross section for the Pb target, obtained by subtracting the nuclear contribution scaled from the C target spectrum in (a). The spectrum is compared with the calculations for the possible single-particle configurations described in the text.

We analyzed the Coulomb dissociation spectrum with a conventional equivalent photon method [9,10]. Here, the Coulomb dissociation spectrum is related to the $B(E1)$ distribution $dB(E1)/dE_{\rm rel}$ as in

$$\frac{d\sigma_{\rm CD}}{dE_{\rm rel}} = \frac{16\pi^3}{9\hbar c} N_{E1}(E_{\rm x}) \frac{dB(E1)}{dE_{\rm rel}}, \qquad (1)$$

where $N_{E1}(E_{\rm x})$ represents the number of virtual photons for $E1$ excitation. Within the framework of a direct breakup mechanism [3,11,12,21,22], the $B(E1)$ distribution is simply given by the transition matrix element

$$\frac{dB(E1)}{dE_{\rm rel}} = \left| \langle \mathbf{q} | \frac{Ze}{A} r Y^1_m | \Phi(\mathbf{r}) \rangle \right|^2 . \qquad (2)$$

The wave function $\Phi(\mathbf{r})$ stands for ^{19}C in the ground state, and is represented by a product of the radial part $R(r)$ and the angular part of the single valence neutron. The $E1$ operator involves r, the relative distance between the core and valence neutron. The final state $\langle \mathbf{q}|$ describes a neutron in the continuum, well approximated by a plane

wave. With this approximation, the matrix element is a Fourier transform of $rR(r)$.

By comparing the observed spectrum with Eqs. (1) and (2), one can test a wave function for the ground state of ^{19}C. We examined the following configurations, respectively, representing the cases of $J^\pi = 1/2^+$ and $5/2^+$:

$$|^{19}\mathrm{C}(1/2^+)\rangle = \alpha|^{18}\mathrm{C}(0^+) \otimes 2s_{1/2}\rangle + \beta|^{18}\mathrm{C}(2^+) \otimes 1d_{5/2}\rangle,$$

$$|^{19}\mathrm{C}^+(5/2^+)\rangle = \gamma|^{18}\mathrm{C}(2^+) \otimes 2s_{1/2}\rangle + \delta|^{18}\mathrm{C}(0^+) \otimes 1d_{5/2}\rangle,$$

where α, β, γ, and δ denote the spectroscopic amplitude for each configuration. These configurations are selected on the basis of shell model calculations [14,15]. Arguments concerning a possible $J^\pi = 3/2^+$ configuration are essentially the same as for $J^\pi = 5/2^+$, as shown in the theoretical work on the Coulomb dissociation [16].

The excitation energy spectrum was calculated using radial wave functions of single particles, which were derived from a Woods-Saxon potential with parameters $r_0 = 1.236$ fm, $a = 0.62$ fm, and $V_{so} = 7.0$ MeV (spin-orbit strength). The results were not sensitive to the choice of these parameters. In the following comparison, we neglect the $^{18}\mathrm{C}(2^+) \otimes 1d_{5/2}$ term for the $J^\pi = 1/2^+$, which makes only a negligible contribution to the matrix element due to the centrifugal barrier for the $1d_{5/2}$ orbital and to the larger separation energy by 1.62 MeV for this component of core excitation.

The results of our calculations are compared with the observed spectrum in Fig. 1(b). The dotted line corresponds to the component relevant to α for the $J^\pi = 1/2^+$ case. The dot-dashed and dashed lines, respectively, correspond to the components of γ and δ for the $J^\pi = 5/2^+$ case. All these lines were calculated by using $S_n = 160$ keV (adopted value). The experimental resolutions and possible reacceleration effects, as estimated by Monte Carlo simulations, are included by convoluting the Gaussian distribution with a width of $\Delta E = 0.24\sqrt{E_{\mathrm{rel}}}$ MeV. This convolution has a negligible effect on the original spectral shape.

The calculated spectral shape is very different for the $J^\pi = 1/2^+$ and $J^\pi = 5/2^+$ cases. For $J^\pi = 5/2^+$, any mixture of the two components failed to reproduce the data despite varying S_n in a wide range (from 100 to 700 keV). Most noticeably, the calculation could not account for the magnitude of the cross section. As indicated by the dot-dashed (dashed) lines, the calculated peak cross section greatly underpredicted the experimental result even with the maximum spectroscopic strength $\gamma^2(\delta^2) = 1$. On the contrary, the peak height of the spectrum can be reproduced for the case of $J^\pi = 1/2^+$ with $\alpha^2 = 0.064$ (dotted line). However, one needed a further tuning of the S_n value to obtain an overall fit to the spectrum. The lower peak energy and narrower width indicates that the adopted S_n value is too small. A good agreement was obtained using a higher S_n value of 530 keV as shown by the solid line. This S_n value was obtained from an independent analysis described in the next paragraph. In this case a fairly large spectroscopic factor of $\alpha^2 = 0.67$ was deduced. We thus conclude that the ground state of ^{19}C has $J^\pi = 1/2^+$, involving a dominant configuration of $^{18}\mathrm{C}(0^+) \otimes 2s_{1/2}$ and the S_n value of about 500 keV. This configuration is rather close to that predicted by a shell model calculation with the WBP interaction [14,23]. The large amplitude for the s-wave valence neutron and a fairly small S_n value afford a favorable condition for manifestation of a halo structure. The $B(E1)$ strength amounted to $0.71 \pm 0.07\ e^2\,\mathrm{fm}^2$ (1.54 ± 0.15 W.u.), a large strength typical for a halo nucleus. Indeed the strength corresponds to an extended radius of the valence neutron as large as $\sqrt{\langle r^2\rangle} = 5.5 \pm 0.3$ fm, deduced by using the $E1$ sum rule for a decoupled neutron [24]. Combining this $\sqrt{\langle r^2\rangle}$ value with the ^{18}C core radius, we can estimate the rms radius of ^{19}C to be 3.0 ± 0.1 fm, which is consistent with that extracted from the interaction cross section measurement [25].

We now show that the S_n value can be determined from an analysis of the angular distribution of ^{19}C (i.e., ^{18}C + n center of mass). Since we measured the momentum vectors of incident ^{19}C, outgoing ^{18}C, and neutron in coincidence, one can determine the deflection angle θ_{D} on an event by event basis. The angular distribution is described as

$$\frac{d\sigma(\theta_{\mathrm{D}}, E_{\mathrm{x}})}{d\Omega} \propto \frac{dN_{E1}(\theta_{\mathrm{D}}, E_{\mathrm{x}})}{d\Omega} B(E1; E_{\mathrm{x}}). \qquad (3)$$

Note that the angular distribution is solely dictated by the $E1$ virtual photon number ($dN_{E1}/d\Omega$). In turn, the pattern of $dN_{E1}/d\Omega$ is determined by the value of $E_{\mathrm{x}}(= E_{\mathrm{rel}} + S_n)$. Thus for a given E_{rel}, the angular

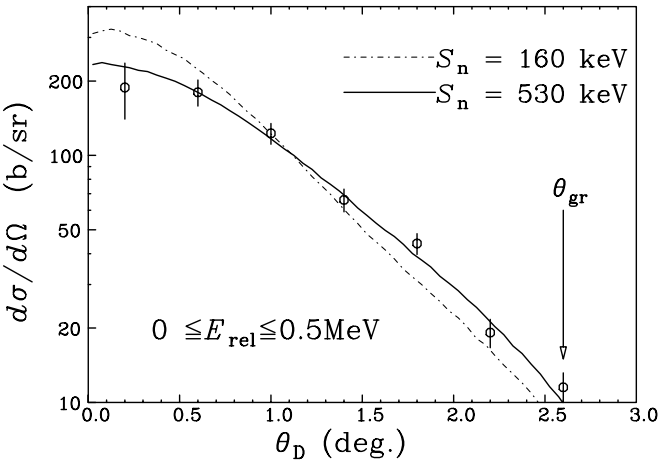

FIG. 2. Angular distribution of ^{18}C + n c.m. system on a Pb target. The angular distribution is obtained as a function of the c.m. angle of ^{19}C + Pb. θ_{gr} represents the grazing angle (2.6°). The curves are calculations for $S_n = 530$ keV (solid curve, best fit), and 160 keV (dot-dashed curve, adopted S_n value [13]).

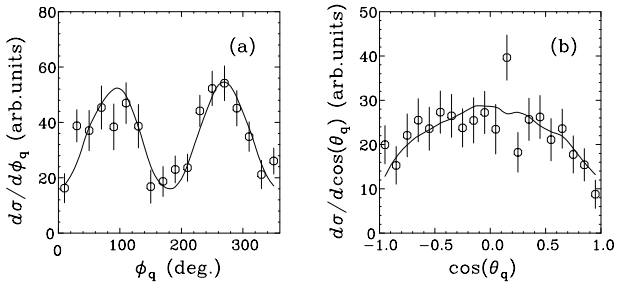

FIG. 3. Azimuthal (a) and polar (b) angular distributions of ^{18}C in the ^{18}C + n rest frame. The solid curves represent the estimation based on a first order perturbation theory for $E1$ excitation.

distribution is controlled by a parameter S_n and is independent of the choice for the final state wave function. Hence S_n was extracted from the measured angular distribution rather than the relative energy spectrum shown in Fig. 1. Note that the result from this method is independent of the possible existence of a low-lying resonance [26]. Figure 2 shows the obtained angular distribution for $0 \leq E_{\rm rel} \leq 0.5$ MeV in comparison with the calculated spectra. Here, an angular resolution of 8.4 mrad (in 1σ) was folded in the calculated spectra. The angular distribution was best fitted with $S_n = 530 \pm 130$ keV as indicated by the solid curve in Fig. 2, while the adopted value $S_n = 160$ keV was unable to reproduce the angular distribution. Here, the estimated error refers to one unit deviation of χ^2. The reduced χ^2 for 530 keV is 0.69, indicating a reasonable fit. Note that the size of uncertainty in S_n is to be compared with $E_{\rm x}$, not with the total mass of ^{19}C.

To complete the experimental analysis, the $E1$ dominance in the observed dissociation was examined by observing the angular correlations (the angular distribution of a breakup particle, ^{18}C, seen in the rest frame of the ^{18}C + n outgoing system), as shown in Fig. 3. This method for determining the multipolarity is based on a first order perturbation theory [21,22,27], and was applied for ^{11}Be [3]. The coordinate system is defined by the z axis pointing to the direction of the outgoing ^{18}C + n center of mass. This direction is almost identical to the axis of the projectile velocity. The y axis is in the reaction plane and the x axis is perpendicular to the reaction plane. Figure 3 shows the spectra for the azimuthal angle (ϕ_q) (a), and polar angle (θ_q) (b). These spectra were obtained for $0 \leq E_{\rm rel} \leq 1$ MeV and $1^\circ \leq \theta_{\rm D} \leq 3^\circ$. The spectra are consistent with the $E1$ patterns as indicated by the solid curves calculated with the first order perturbation theory for $E1$ excitation.

In conclusion, we made a kinematically complete measurement of ^{19}C Coulomb dissociation. A large $E1$ cross section with a peak $E_{\rm rel} \cong 300$ keV was observed. From the data, a $J^\pi = 5/2^+$ ground state configuration of ^{19}C was excluded. A $J^\pi = 1/2^+$ ground state with a dominant $^{18}{\rm C}(0^+) \otimes 2s_{1/2}$ configuration with $S_n = 530 \pm 130$ keV reproduced the data very well. This S_n value was derived independently from the analysis of the angular distribution of the ^{18}C + n center of mass system. The dominance of a loosely bound $2s_{1/2}$ neutron demonstrates that the ^{19}C provides another good case for a one-neutron halo nucleus.

Sincere gratitude is extended to the accelerator staff of RIKEN for their excellent operation of the beam delivery. We also thank B. Sherrill and A. Navin for their valuable comments.

*Present address: NSCL, Michigan State University, East Lansing, MI 48824.
†Present address: ENEA, Applied Physics Division, Via Don Fiammelli 2, 40129 Bologna, Italy.

[1] P. G. Hansen, A. S. Jensen, and B. Jonson, Annu. Rev. Nucl. Part. Sci. **45**, 591 (1995), and references therein.
[2] I. Tanihata, Prog. Part. Nucl. Phys. **35**, 505 (1995), and references therein.
[3] T. Nakamura *et al.*, Phys. Lett. B **331**, 296 (1994).
[4] R. Anne *et al.*, Phys. Lett. B **304**, 55 (1993); R. Anne *et al.*, Nucl. Phys. **A575**, 125 (1994).
[5] T. Kobayashi *et al.*, Phys. Lett. B **232**, 51 (1989).
[6] K. Ieki *et al.*, Phys. Rev. Lett. **70**, 730 (1993); D. Sackett *et al.*, Phys. Rev. C **48**, 118 (1993).
[7] S. Shimoura *et al.*, Phys. Lett. B **348**, 29 (1995).
[8] M. Zinser *et al.*, Nucl. Phys. **A619**, 151 (1997).
[9] J. D. Jackson, *Classical Electrodynamics* (Wiley, New York, 1975), 2nd ed.
[10] C. Bertulani and G. Baur, Phys. Rep. **163**, 299 (1988).
[11] T. Otsuka *et al.*, Phys. Rev. C **49**, 2289R (1994).
[12] A. Mengoni *et al.*, in *Proceedings of the International Symposium on Capture Gamma-ray and Related Topics*, edited by G. L. Molnar, T. Belgya, and Zs. Revay, (Springer, New York, 1977), p. 416.
[13] G. Audi and A. H. Wapstra, Nucl. Phys. **A565**, 1 (1993); G. Audi, A. H. Wapstra, and M. Dedieu, Nucl. Phys. **A565**, 193 (1993), and references therein.
[14] D. Bazin *et al.*, Phys. Rev. Lett. **74**, 3569 (1995).
[15] D. Bazin *et al.*, Phys. Rev. C **57**, 2156 (1998).
[16] D. Ridikas *et al.*, Nucl. Phys. **A628**, 363 (1998).
[17] T. Baumann *et al.*, Phys. Lett. B **439**, 256 (1998).
[18] F. M. Marqués *et al.*, Phys. Lett. B **381**, 407 (1996).
[19] T. Aumann *et al.*, Phys. Rev. C **59**, 1252 (1999).
[20] T. Kubo *et al.*, Nucl. Instrum. Methods Phys. Res., Sect. B **70**, 309 (1992).
[21] C. A. Bertulani and L. F. Canto, Nucl. Phys. **A539**, 163 (1992).
[22] G. Baur, C. A. Bertulani, and D. M. Kalassa, Nucl. Phys. **A550**, 527 (1992).
[23] E. K. Warburton and B. A. Brown, Phys. Rev. C **46**, 923 (1992).
[24] H. Esbensen and G. Bertsch, Nucl. Phys. **A542**, 310 (1992).
[25] A. Ozawa *et al.*, RIKEN Report No. RIKEN-AF-NP-294, 1998.
[26] M. H. Smedberg and M. V. Zhukov, Phys. Rev. C **59**, 2048 (1999).
[27] H. Esbensen and G. Bertsch, Nucl. Phys. **A600**, 37 (1996).